Cell Death and Differentiation (2013) 20, 1580–1592

www.nature.com/cdd

TNFR1 determines progression of chronic liver injury in the IKKγ/Nemo genetic model

FJ Cubero[1,5], A Singh[1,5], E Borkham-Kamphorst[2], YA Nevzorova[1], M Al Masaoudi[1], U Haas[2], MV Boekschoten[3], N Gassler[4], R Weiskirchen[2], M Muller[3], C Liedtke[1] and C Trautwein*[,1]

Death receptor-mediated hepatocyte apoptosis is implicated in a wide range of liver diseases including viral and alcoholic hepatitis, ischemia/reperfusion injury, fulminant hepatic failure, cholestatic liver injury, as well as cancer. Deletion of NF-κB essential modulator in hepatocytes (IKKγ/Nemo) causes spontaneous progression of TNF-mediated chronic hepatitis to hepatocellular carcinoma (HCC). Thus, we analyzed the role of death receptors including TNFR1 and TRAIL in the regulation of cell death and the progression of liver injury in IKKγ/Nemo-deleted livers. We crossed hepatocyte-specific IKKγ/Nemo knockout mice (Nemo$^{\Delta hepa}$) with constitutive TNFR1$^{-/-}$ and TRAIL$^{-/-}$ mice. Deletion of TNFR1, but not TRAIL, decreased apoptotic cell death, compensatory proliferation, liver fibrogenesis, infiltration of immune cells as well as pro-inflammatory cytokines, and indicators of tumor growth during the progression of chronic liver injury. These events were associated with diminished JNK activation. In contrast, deletion of TNFR1 in bone-marrow-derived cells promoted chronic liver injury. Our data demonstrate that TNF- and not TRAIL signaling determines the progression of IKKγ/Nemo-dependent chronic hepatitis. Additionally, we show that TNFR1 in hepatocytes and immune cells have different roles in chronic liver injury–a finding that has direct implications for treating chronic liver disease.

Cell Death and Differentiation (2013) **20,** 1580–1592; doi:10.1038/cdd.2013.112; published online 9 August 2013

The nuclear factor (NF)-κB signaling pathway mediates a variety of important cellular functions by regulating immune and inflammatory responses.[1,2] NF-κB transcription factors are kept inactive in the cytoplasm through binding to members of the IκB family of inhibitory proteins. Upon stimulation, NF-κB translocates into the nucleus, where it activates pro-inflammatory target genes. IKKγ/Nemo is the essential regulatory unit of the IKK complex. Deletion of IKKγ/Nemo is lethal during embryonic development, as mice die from hepatocyte apoptosis.[3–7] Futhermore, hepatocyte-specific IKKγ/Nemo knockout mice (Nemo$^{\Delta hepa}$) are highly susceptible to TNF-mediated spontaneous cell death.[8]

Recent work by our group demonstrated that apoptosis is blocked in Nemo$^{\Delta hepa}$/Caspase8$^{\Delta hepa}$ double knockout animals, suggesting that apoptosis is Caspase-8 (Casp8)-dependent in Nemo$^{\Delta hepa}$ mice.[9] These results implicate that death receptors have a pivotal role in the complex regulation, leading to hepatocyte apoptosis in Nemo$^{\Delta hepa}$ mice.

Among others, death receptors include TNFR1 and TRAIL receptors 1 and 2 (TRAIL-R1/DR4 and TRAIL-R2/DR5).[10] Lethal hepatocyte apoptosis observed in p65 knockout mice can be rescued by crossing these mice into a TNF or TNFR1-null background.[11,12] However, TNFR1/p65 double-knockout mice die shortly after birth because of massive acute inflammation of the liver. Furthermore, Nemo$^{\Delta hepa}$ mice overexpress the TRAIL-specific death receptor DR5 and TRAIL-expressing NK cells are activated in Nemo$^{\Delta hepa}$ livers.[13]

To specifically address the progression of TNF-mediated chronic liver injury and to define the impact of death receptor-mediated signaling, we questioned whether the deletion of TNFR1 or TRAIL/DR5 in a genetic model of chronic liver disease, the Nemo$^{\Delta hepa}$ mice, could have an impact on liver injury. Here, we demonstrate that the death receptor TNFR1 in hepatocytes and immune cells has different roles in the progression of liver injury in Nemo$^{\Delta hepa}$ mice.

[1]Department of Internal Medicine III, University Hospital, RWTH Aachen, Aachen, Germany; [2]Institute of Clinical Chemistry and Pathobiochemistry, University Hospital, RWTH Aachen, Aachen, Germany; [3]Division of Human Nutrition, Metabolism and Genomics, Wageningen University, Wageningen, The Netherlands and [4]Institute of Pathology, University Hospital, RWTH Aachen, Germany

*Corresponding author: C Trautwein, Department of Internal Medicine III, University Hospital, RWTH Aachen, Pauwelstraße, 30, Aachen 52074, Germany. Tel: +49 241 80 80866; Fax: +49 241 80 82455; E-mail: ctrautwein@ukaachen.de

[5]These authors contributed equally to this work.

Keywords: TNFR1; TRAIL; IKKγ/Nemo; hepatitis

Abbreviations: ALT, alanine aminotransferase; AP, alkaline phosphatase; ASH, Alcoholic steatohepatitis; BAMBI, bone morphogenic protein and activin membrane-bound inhibitor; BMT, bone marrow transplantation; BrdU, Bromodeoxyuridine; DAPI, 4′,6′-diamidino-2-phenylindole; DEN, diethylnitrosamine; DR6, Death Receptor signaling-6; FGL1, fibrinogen-like protein 1; HCC, hepatocellular carcinoma; KC, Kupffer cells; IKKγ/Nemo, essential regulatory subunit of the IKK complex; IL-6, interleukin-6; LY96, lymphocyte antigen-96; MCD, methionine and choline-deficient; NASH, non-alcoholic steatohepatitis; Nemo$^{\Delta hepa}$, hepatocyte-specific deletion of IKKγ/Nemo; NF-κBie, nuclear factor of kappa light polypeptide gene enhancer in B-cells inhibitor; NK, natural killer cells; ORM2, orosomucoid-2; PCNA, Proliferating Cell Nuclear Antigen; qRT-PCR, quantitative real-time polymerase chain reaction; TNFR1, Tumor Necrosis Factor Receptor-1; TRAIL, Tumor Necrosis Factor (TNF)-Related Apoptosis-Inducing Ligand; SAA2, Serum Amyloid-A$_2$; SCD2, stearoyl-Coenzyme A desaturase 2; α-SMA, alpha-smooth-muscle actin; SMAD3, MAD homolog 3; SOCS3, Suppressor of cytokine signaling 3; STAT3, signal transducer and activator of transcription-3; TAK1, TGFβ-activated kinase-1; TLR4, Toll-like Receptor-4

Received 13.3.13; revised 18.6.13; accepted 12.7.13; Edited by A Ashkenazi; published online 09.8.13

Results

Deletion of TNFR1 decreases TNF-mediated hepato cellular damage. Hepatocytes with the deletion of IKKγ/Nemo show hypersensitivity against TRAIL and TNF.[13] Loss of Casp8 in Nemo$^{\Delta hepa}$ mice prevents liver apoptosis and disease progression.[9] As TNF receptor family members are upstream mediators of Casp8-dependent apoptosis, we aimed to define death receptors critically involved in mediating the function of IKKγ/Nemo in cell death. Thus, we tested the relevance of the TNFR1 pathway for disease progression by generating Nemo$^{\Delta hepa}$/TNFR1$^{-/-}$ double-knockout mice and compared them with Nemo$^{\Delta hepa}$/TRAIL$^{-/-}$ and Nemo$^{\Delta hepa}$ mice.

Macroscopically, livers from 8-week-old Nemo$^{\Delta hepa}$ and Nemo$^{\Delta hepa}$/TRAIL$^{-/-}$ appeared similar and were characterized by widespread lesions. In contrast, no remarkable lesions were observed in Nemo$^{\Delta hepa}$/TNFR1$^{-/-}$ animals and WT controls (Figure 1a, upper panel, Supplementary Figures 1a and b). Liver histology of Nemo$^{\Delta hepa}$ and Nemo$^{\Delta hepa}$/TRAIL$^{-/-}$ mice was characterized by a strong inflammatory response of the liver parenchyma associated with fat accumulation in hepatocytes. Basal hepatitis and steatosis were dependent on functional TNF signaling, as it was significantly reduced in Nemo$^{\Delta hepa}$/TNFR1$^{-/-}$ livers (Figure 1a, lower panel). Furthermore, we analyzed lipid deposition in the livers of these mice by means of Oil-Red-O staining. Our results confirmed that fat accumulation was considerably diminished in livers of Nemo$^{\Delta hepa}$/TNFR1$^{-/-}$ compared with Nemo$^{\Delta hepa}$ and Nemo$^{\Delta hepa}$/TRAIL$^{-/-}$ mice (Supplementary Figure 1A). Moreover, 8-week-old Nemo$^{\Delta hepa}$/TNFR1$^{-/-}$ mice displayed a considerable decrease in serum ALT levels when compared with Nemo$^{\Delta hepa}$ and Nemo$^{\Delta hepa}$/TRAIL$^{-/-}$ animals (Figure 1b).

Nemo$^{\Delta hepa}$ mice develop spontaneous hepatocyte apoptosis, considered to be a critical mediator of disease progression. Genetic TNFR1 inactivation in Nemo$^{\Delta hepa}$ livers significantly reduced hepatic apoptosis compared with Nemo$^{\Delta hepa}$ and Nemo$^{\Delta hepa}$/TRAIL$^{-/-}$ livers as evidenced by diminished Caspase-3 cleavage, Caspases 3 and 8 activity and TUNEL analysis, respectively (Figures 1c–e). Next, we tested the effect of TNFR1 deletion in Nemo$^{\Delta hepa}$ hepatocytes *in vitro.* Primary hepatocytes were isolated and cultured for 8 h (Supplementary Figure 1c). Our first results showed that the viability of Nemo$^{\Delta hepa}$ hepatocytes was significantly improved after TNFR1 deletion as determined by light microscopy and MTT survival assay (Supplementary Figures 1d and e). Thus, we performed apoptosis-specific FACS analysis using Annexin V/FITC staining in Nemo$^{\Delta hepa}$ primary hepatocytes 8 h after plating. As controls, primary hepatocytes derived from WT and Nemo$^{\Delta hepa}$/Casp8$^{\Delta hepa}$ mice were included. Nemo$^{\Delta hepa}$ cells showed strong increase in Annexin V staining compared with WT hepatocytes, whereas the signal was decreased after TNFR1 deletion. Indeed, Nemo$^{\Delta hepa}$/TNFR1$^{-/-}$, and more prominently Nemo$^{\Delta hepa}$/Casp8$^{\Delta hepa}$ hepatocytes, exhibited less apoptosis (Figure 1f). Accordingly, our results suggest that TNFR1 in hepatocytes significantly contributes to apoptosis of Nemo-deficient cells.

Ablation of TNFR1 in Nemo$^{\Delta hepa}$ liver results in reduced compensatory proliferation and liver fibrogenesis. Chronic liver injury in Nemo$^{\Delta hepa}$ livers triggers compensatory proliferation associated with hepatocellular carcinoma (HCC) development.[8] Therefore, we tested whether the deletion of TNFR1 or TRAIL would have an effect on cell proliferation in IKKγ/Nemo-deficient livers. By using cell cycle markers for total cell cycle activity (Ki-67), S-phase progression (BrdU incorporation, Cyclin A) and G1/S-phase transition (PCNA), we found a significant decline in cell cycle activity in Nemo$^{\Delta hepa}$/TNFR1$^{-/-}$ livers. In contrast, no difference in cell proliferation was observed between Nemo$^{\Delta hepa}$ and Nemo$^{\Delta hepa}$/TRAIL$^{-/-}$ mice (Figures 2a–c, Supplementary Figures 2A–D).

Nemo$^{\Delta hepa}$ livers revealed increased expression of the cell cycle inhibitor p21, which is induced by liver injury or DNA damage.[14] Unexpectedly, p21 mRNA and protein expression levels were significantly decreased in Nemo$^{\Delta hepa}$/TNFR1$^{-/-}$ livers compared with Nemo$^{\Delta hepa}$ and Nemo$^{\Delta hepa}$/TRAIL$^{-/-}$ cohorts (Figure 2c).

Subsequently, we aimed to investigate whether the development of liver fibrosis observed in Nemo$^{\Delta hepa}$ mice could be attenuated by simultaneous inactivation of TNFR1. We measured hepatic fiber formation by Sirius red staining and determined additional pro-fibrotic markers such as Collagen IA1, alpha-smooth-muscle actin (α-SMA) and hydroxyprolin. Livers from 13-week-old Nemo$^{\Delta hepa}$/TNFR1$^{-/-}$ mice showed significantly less Sirius red-positive area compared with Nemo$^{\Delta hepa}$ and Nemo$^{\Delta hepa}$/TRAIL$^{-/-}$ livers (Figure 2d).

These results were corroborated by alleviated induction of Collagen IA1 (Figure 2e, Supplementary Figure 2E) and reduced α-SMA expression in Nemo$^{\Delta hepa}$/TNFR1$^{-/-}$ compared with Nemo$^{\Delta hepa}$ and Nemo$^{\Delta hepa}$/TRAIL$^{-/-}$ livers (Figure 2e, Supplementary Figure 2F). Altogether, these results demonstrate that compensatory proliferation and development of liver fibrosis are reduced after the deletion of TNFR1 in Nemo$^{\Delta hepa}$ mice.

Immune-cell infiltration and pro-inflammatory cytokines are decreased in Nemo$^{\Delta hepa}$/TNFR1$^{-/-}$ livers. The infiltration of distinct immune-cell populations directed by chemotactic cytokines is a central pathogenic feature following chronic liver injury.[15] Thus, we characterized the hepatic inflammatory cell populations by the FACS analysis. F4/80^{+}-macrophages, CD11b^{+}/Ly6G^{+}-neutrophils and CD45^{+}-lymphoid cells were significantly increased in Nemo$^{\Delta hepa}$ and Nemo$^{\Delta hepa}$/TRAIL$^{-/-}$ compared with WT and Nemo$^{\Delta hepa}$/TNFR1$^{-/-}$ livers (Figures 3a–c, Supplementary Figures 3A–C). These findings were further confirmed by immunofluorescence stainings of liver cryosections (Supplementary Figures 3B and C).

To test whether decreased liver injury after the deletion of TNFR1 in IKKγ/Nemo mice influenced the expression of pro-inflammatory cytokines, we performed qRT-PCR. IFN-γ, IL-1ß and TNF mRNA levels were significantly reduced in Nemo$^{\Delta hepa}$/TNFR1$^{-/-}$ compared with Nemo$^{\Delta hepa}$ livers (Figures 3d–f). Moreover, whereas Nemo$^{\Delta hepa}$/TNFR1$^{-/-}$ elicited the lack of TNFR1 expression, Nemo$^{\Delta hepa}$/TRAIL$^{-/-}$ displayed increased protein levels (Supplementary Figure 3D).

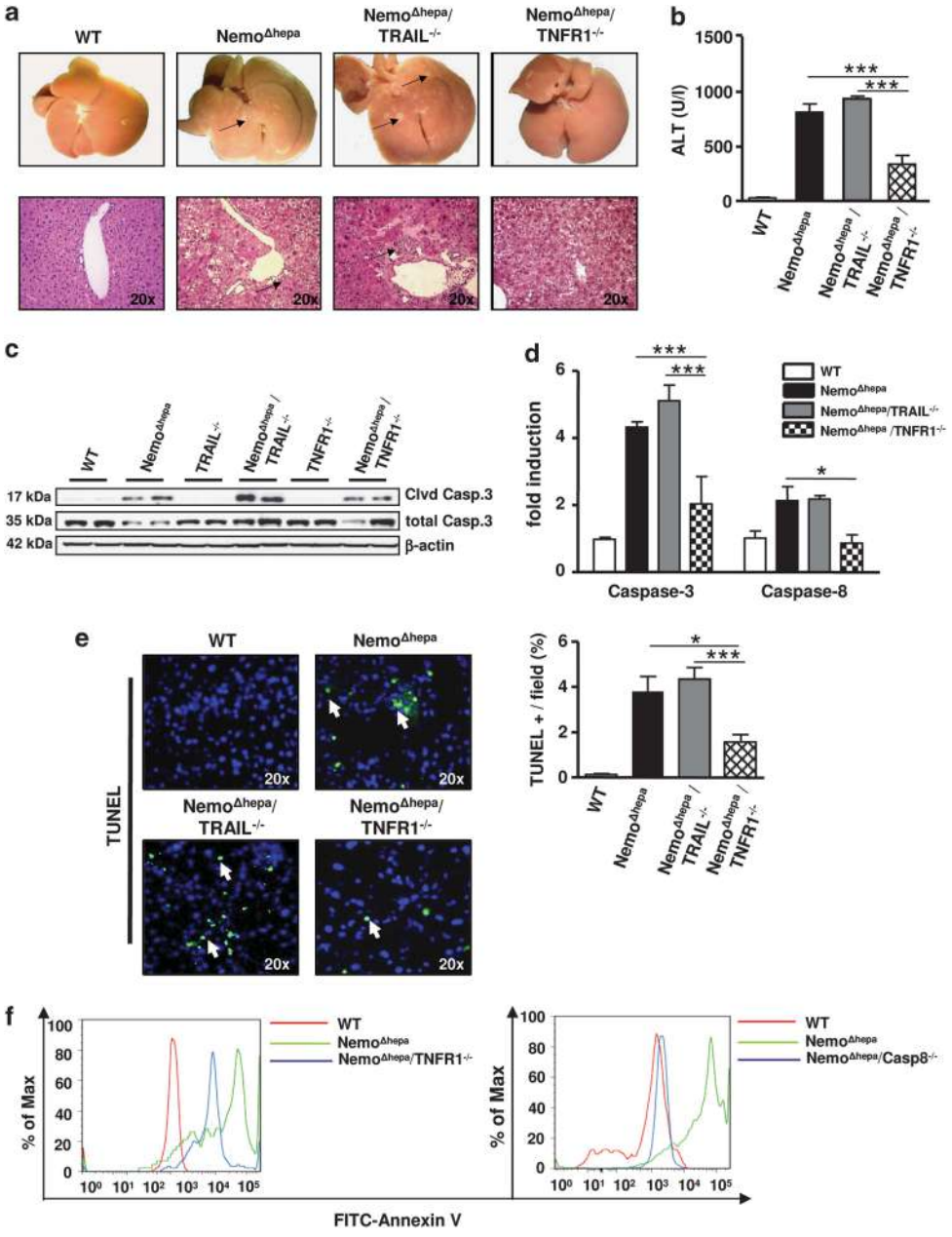

Figure 1 TNFR1 deletion reduces hepatocellular death of Nemo-deficient hepatocytes. (**a**) Macroscopic appearance of livers of WT, Nemo$^{\Delta hepa}$, Nemo$^{\Delta hepa}$/TRAIL$^{-/-}$ and Nemo$^{\Delta hepa}$/TNFR1$^{-/-}$ mice at 8 weeks of age. Arrows indicate widespread lesions (upper panel). Representative H/E staining of liver sections of 8-week-old animals. Arrows indicate cell infiltration (lower panel). (**b**) Serum ALT levels of 8-week-old WT, Nemo$^{\Delta hepa}$, Nemo$^{\Delta hepa}$/TNFR1$^{-/-}$ and Nemo$^{\Delta hepa}$/TRAIL$^{-/-}$ mice were determined. Results are expressed as mean; error bars indicate S.E.M. ($n=6$, $P<0.001$). (**c**) Immunoblot analysis of liver extracts from 8-week-old mice using antibodies against cleaved Caspase-3, total Caspase-3 and β-actin as loading control. (**d**) Caspase-3 and Caspase-8 activities in 8-week-old WT, Nemo$^{\Delta hepa}$, Nemo$^{\Delta hepa}$/TRAIL$^{-/-}$ and Nemo$^{\Delta hepa}$/TNFR1$^{-/-}$ mice. Activity is represented as fold induction over untreated controls. (**e**) Representative TUNEL staining of liver sections from 8-week-old WT, Nemo$^{\Delta hepa}$, Nemo$^{\Delta hepa}$/TRAIL$^{-/-}$ and Nemo$^{\Delta hepa}$/TNFR1$^{-/-}$ mice. Apoptotic cells are stained in green and highlighted by arrows. TUNEL-positive cells in the livers of 8-week-old WT, Nemo$^{\Delta hepa}$, Nemo$^{\Delta hepa}$/TRAIL$^{-/-}$ and Nemo$^{\Delta hepa}$/TNFR1$^{-/-}$ mice were quantified ($n=6$, $^{*}P<0.05$; $^{***}P<0.001$). (**f**) Representative FACS blots of primary isolated hepatocytes from WT (red), Nemo$^{\Delta hepa}$ (blue), Nemo$^{\Delta hepa}$/TNFR1$^{-/-}$ (green) and Nemo$^{\Delta hepa}$/Casp8$^{-/-}$ (blue), and stained with Annexin V/FITC antibody *versus* percentage of total population ($n=4$)

These results demonstrate that attenuated liver injury after TNFR1$^{-/-}$ deletion in Nemo$^{\Delta hepa}$ livers reduces cell infiltration and expression of pro-inflammatory cytokines.

TNFR1 triggers the activation of pro-inflammatory genes in IKKγ/Nemo-deficient livers. To investigate the underlying molecular mechanisms conferring protection in Nemo$^{\Delta hepa}$/TNFR1$^{-/-}$ livers, we next performed whole-liver genome microarray to identify potential differences in target gene expression between the knockout strains compared with WT mice (Figure 4a). The overlap of top upregulated or downregulated genes in the liver elicited differential clustering between Nemo$^{\Delta hepa}$ and Nemo$^{\Delta hepa}$/TRAIL$^{-/-}$ livers from those of Nemo$^{\Delta hepa}$/TNFR1$^{-/-}$ and

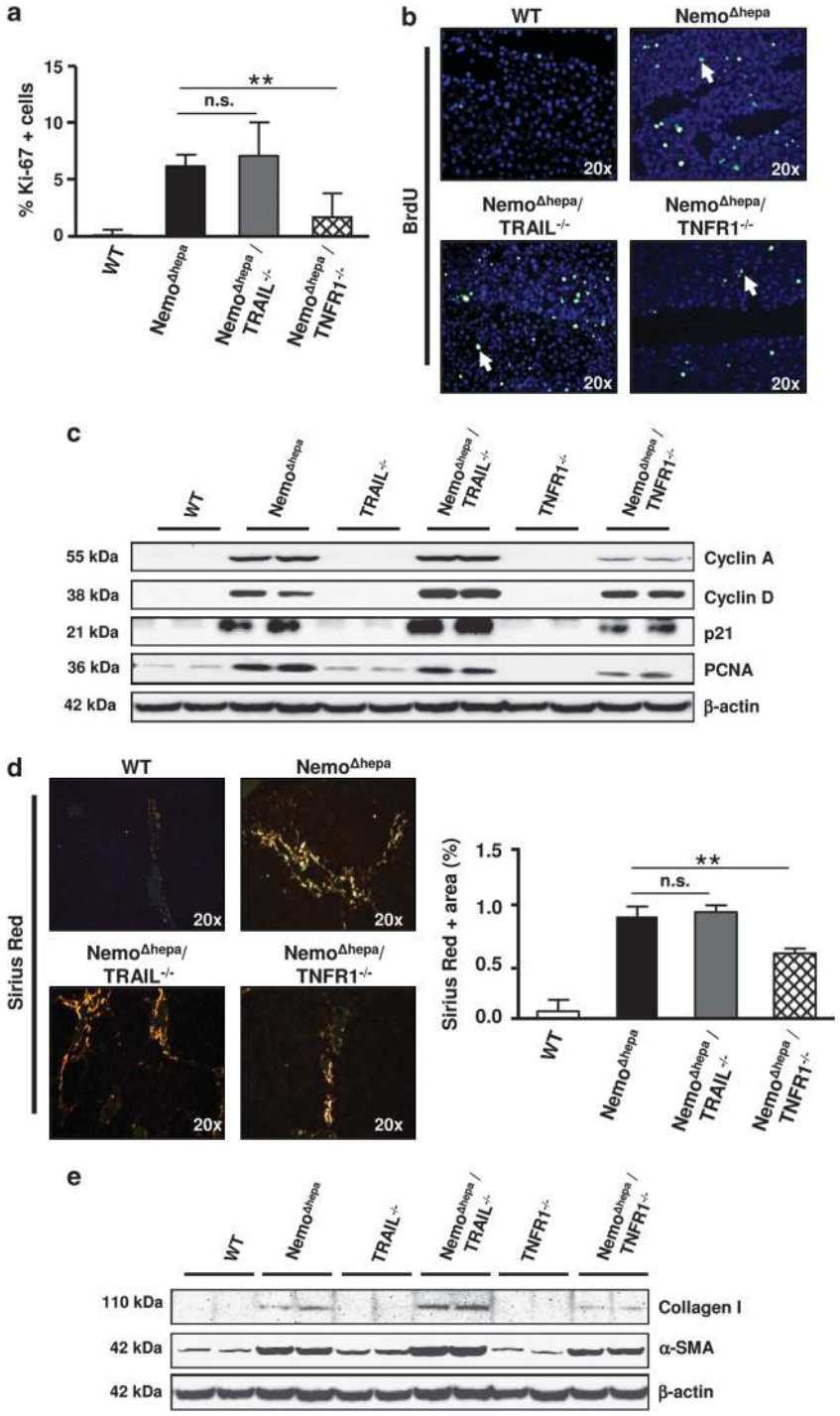

Figure 2 Ablation of TNFR1 in Nemo$^{\Delta hepa}$ liver results in reduced compensatory proliferation and liver fibrogenesis. (**a**) Proliferation was quantified by the determination of Ki-67-positive cells per high-magnification fields ($n=4$; 5 fields per animal; $^{**}P<0.01$). (**b**) Bromodeoxyuridine (BrdU) uptake (green) in livers of WT, Nemo$^{\Delta hepa}$ and Nemo$^{\Delta hepa}$/TRAIL$^{-/-}$ and Nemo$^{\Delta hepa}$/TNFR1$^{-/-}$ mice at 8 weeks of age. Arrows indicate positive BrdU-proliferating cells. (**c**) Western blot for Cyclin A, Cyclin D, p21 and PCNA expression levels was performed in whole protein in whole-liver extracts of WT, Nemo$^{\Delta hepa}$ and Nemo$^{\Delta hepa}$/TRAIL$^{-/-}$ and Nemo$^{\Delta hepa}$ /TNFR1$^{-/-}$ mice. (**d**) Representative photomicrographs of Sirius red staining in paraffin-embedded liver tissue derived from 8-week-old livers of WT, Nemo$^{\Delta hepa}$ and Nemo$^{\Delta hepa}$/TRAIL$^{-/-}$ and Nemo$^{\Delta hepa}$/TNFR1$^{-/-}$ mice. Quantification of Sirius red-positive area was performed using Image J software ($n=4$, $^{**}P<0.01$). (**e**) Liver protein extracts from 8-week-old WT, Nemo$^{\Delta hepa}$ and Nemo$^{\Delta hepa}$/TRAIL$^{-/-}$ and Nemo$^{\Delta hepa}$/TNFR1$^{-/-}$ were prepared and subjected to immunoblot using antibodies detecting Collagen I and α-SMA

Nemo$^{\Delta hepa}$/TRAIL$^{-/-}$/TNFR1$^{-/-}$ mice (Supplementary Figures 4A and B). The array analysis revealed that genes involved in mediating liver fibrosis, hepatic stellate cell activation, acute-phase response, death receptor signaling and hepatic cholestasis were significantly downregulated in Nemo$^{\Delta hepa}$/TNFR1$^{-/-}$ compared with Nemo$^{\Delta hepa}$ and

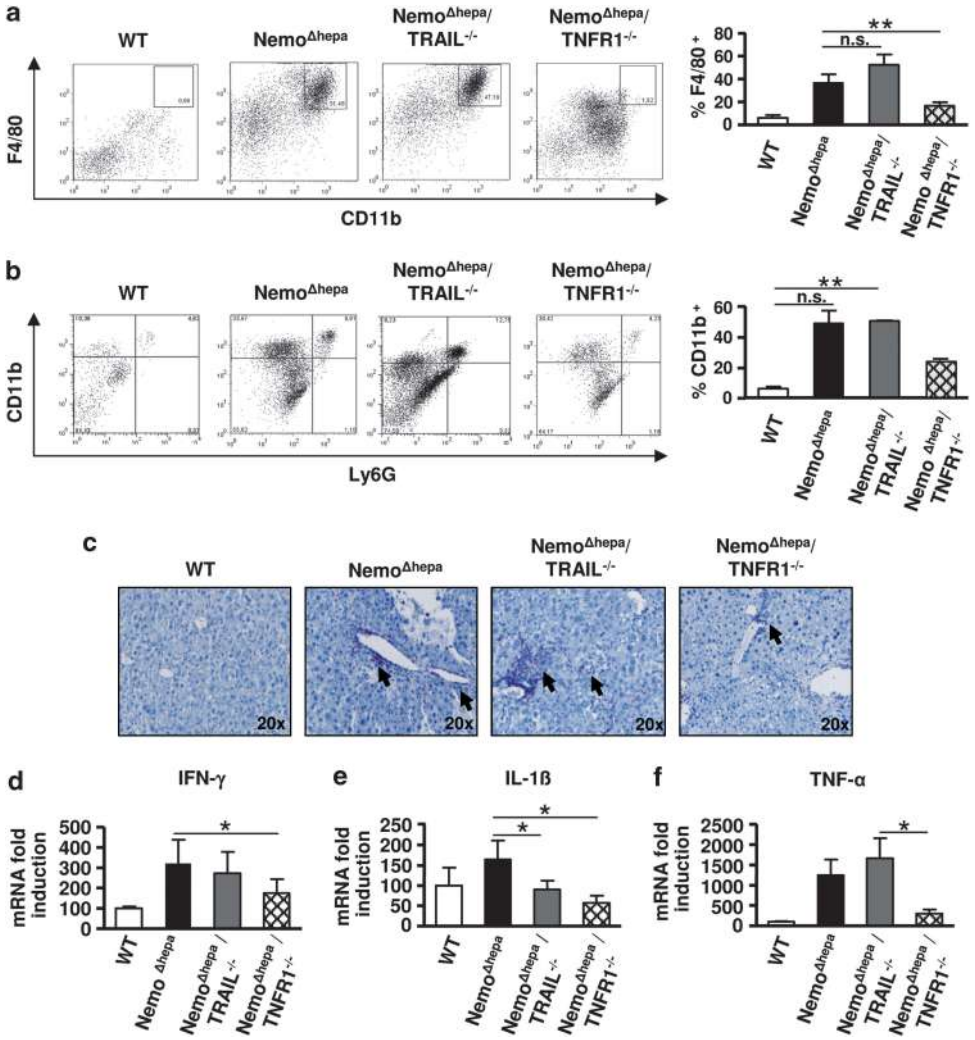

Figure 3 Cell infiltration and inflammation are reduced in Nemo$^{\Delta hepa}$/TNFR1$^{-/-}$ mice. (**a**) Representative FACS blots showing relative number of macrophages and monocytes (CD11b, F4/80) in single liver-cell suspensions derived from WT, Nemo$^{\Delta hepa}$, Nemo$^{\Delta hepa}$/TRAIL$^{-/-}$ and Nemo$^{\Delta hepa}$/TNFR1$^{-/-}$ livers. Quantification of F4/80-positive cells of each mouse strain in the FACS analysis ($n=4$, $^{**}P<0.01$). (**b**) FACS was also performed for the analysis of neutrophils (CD11b, Ly6G) in single liver-cell suspensions derived from WT, Nemo$^{\Delta hepa}$, Nemo$^{\Delta hepa}$/TRAIL$^{-/-}$ and Nemo$^{\Delta hepa}$/TNFR1$^{-/-}$ livers. Percentage of CD11b-positive cells of each mouse strain in the FACS analysis ($n=4$, $^{**}P<0.01$). (**c**) CD45 staining on paraffin sections was performed in livers of 8 weeks old WT, Nemo$^{\Delta hepa}$, Nemo$^{\Delta hepa}$/TRAIL$^{-/-}$ and Nemo$^{\Delta hepa}$/TNFR1$^{-/-}$ animals. Black arrows denote anti-CD45 positive staining. Quantitative RT-PCR analysis of the mRNA levels of IFN-γ (**d**), IL-1β (**e**) and TNF (**f**), respectively, in the liver of 8-week-old WT, Nemo$^{\Delta hepa}$, Nemo$^{\Delta hepa}$/TRAIL$^{-/-}$ and Nemo$^{\Delta hepa}$/TNFR1$^{-/-}$. Values are mean ± S.E.M. from at least six mice per group ($^*P<0.05$; $^{***}P<0.001$)

Nemo$^{\Delta hepa}$/TRAIL$^{-/-}$ livers (Figure 4a). We selected members of these clusters such as SOCS3, SAA2 and IL-6 (mediators of the acute-phase response) (Figures 4A–C), DR6 (death receptor signaling) and SCD2 (lipid metabolism) (Figure 4a, Supplementary Figures 4C and D), and confirmed the microarray data using qRT-PCR (Figures 4a–c, Supplementary Figures 4C and D). The results showed decreased expression of SOCS3, SAA2, IL-6, DR6 and SCD2 in Nemo$^{\Delta hepa}$/TNFR1$^{-/-}$ livers (Figures 4a–d, Supplementary Figures 4C and D).

To better characterize the relevance of our findings on the activation of intracellular pathways involved in mediating the inflammatory response, we investigated the IL-6/STAT3 pathway. Concomitant with the levels of SOCS3 and SAA2, IL-6 mRNA levels were reduced in Nemo$^{\Delta hepa}$/TNFR1$^{-/-}$ samples (Figures 4b–d). Additionally, we investigated the phosphorylation of STAT3, JNK and JunD in whole-liver extracts (Figures 4e and f). These experiments showed elevated phosphorylation levels of STAT3, JNK and JunD in Nemo$^{\Delta hepa}$ and Nemo$^{\Delta hepa}$/TRAIL$^{-/-}$ livers compared with the respective controls. In contrast, a significant reduction in p-STAT3, p-JNK and p-JunD expression levels was obvious in Nemo$^{\Delta hepa}$/TNFR1$^{-/-}$ livers (Figures 4e and f). Noticeably, p-STAT3 levels were increased in TNFR1 single-knockout animals, a phenomenon which was not observed in Nemo$^{\Delta hepa}$/TNFR1$^{-/-}$ livers.

Hepatocarcinogenesis in Nemo$^{\Delta hepa}$ mice is diminished by blocking TNFR1. Ablation of IKKγ/Nemo in liver parenchymal cells triggers spontaneous HCC development.[8] As TNFR1 and TRAIL deletion differentially affected Nemo$^{\Delta hepa}$-dependent progression of liver injury, we

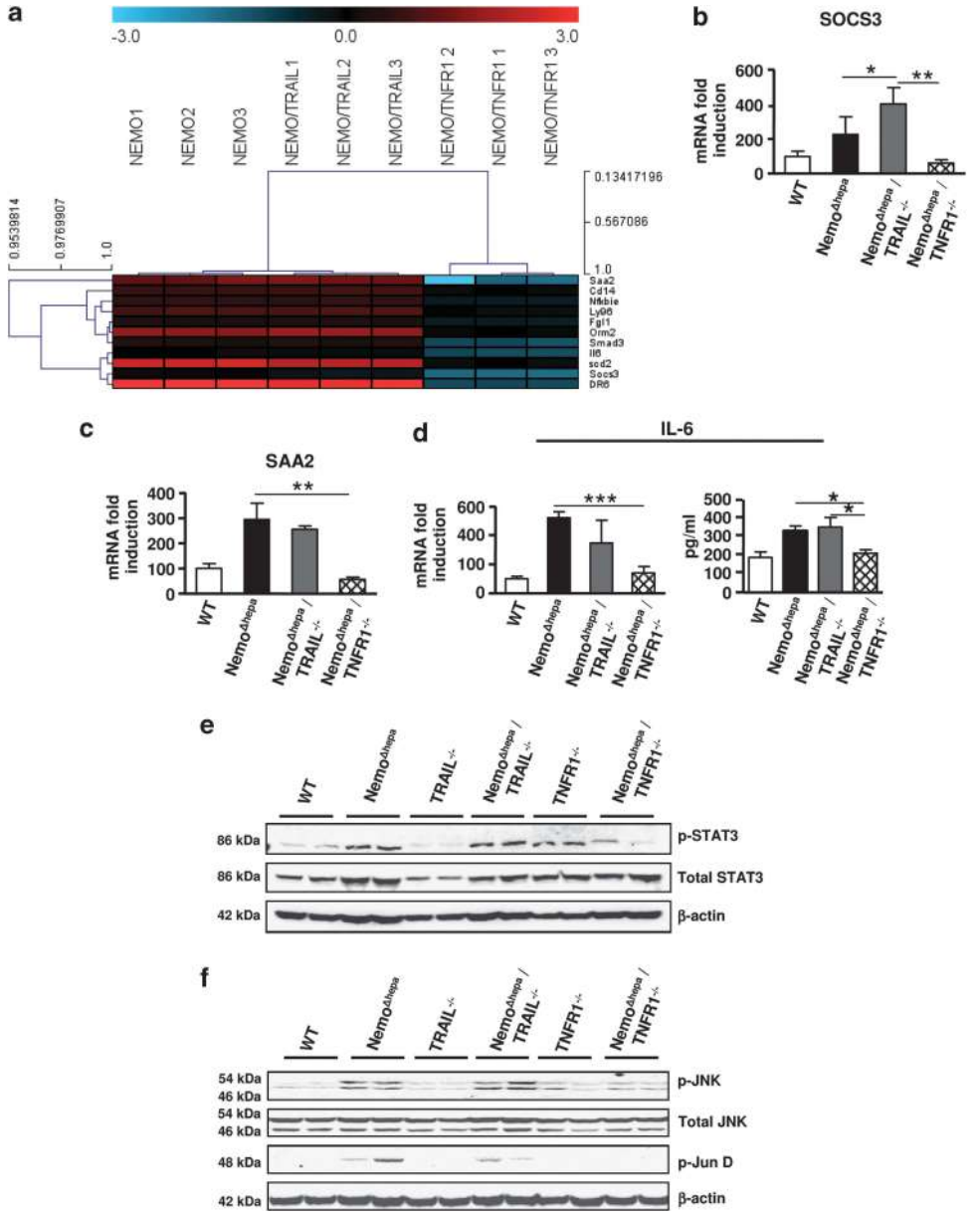

Figure 4 TNFR1 triggers the activation of pro-inflammatory genes in Nemo-deficient livers. (**a**) Gene microarray analysis of 8-week-old liver tissue ($n=3$ livers per group). Red indicates upregulation; blue indicates downregulation compared with WT mice; all genes have an absolute fold change of <1.5. The mRNA expression levels of SOCS3 (**b**), and SAA2 (**c**) and the mRNA and protein expression levels of IL-6 (**d**) were determined by using RT-PCR (left panel) and ELISA (right panel) of liver samples taken from WT, Nemo$^{\Delta hepa}$, Nemo$^{\Delta hepa}$/TRAIL$^{-/-}$ and Nemo$^{\Delta hepa}$/TNFR1$^{-/-}$ mice (*$P<0.05$; **$P<0.01$ and ***$P<0.001$). (**e**) Liver protein extracts from 8-week-old WT, Nemo$^{\Delta hepa}$, Nemo$^{\Delta hepa}$/TRAIL$^{-/-}$ and Nemo$^{\Delta hepa}$/TNFR1$^{-/-}$ were subjected to immunoblotting using antibodies against p-STAT3, and using total STAT3 and β-actin as loading controls. (**f**) The same samples were subjected to immunoblotting using antibodies against p-JNK and p-JunD using β-actin as loading control

investigated the impact on tumor initiation and development in 52-week-old animals. Macroscopically, livers from Nemo$^{\Delta hepa}$ mice revealed both regenerative nodules and large well-defined vascularised nodules resulting in a higher liver weight/body weight ratio compared with WT animals (Figures 5a and b). Although Nemo$^{\Delta hepa}$/TRAIL$^{-/-}$ livers showed a similar phenotype, Nemo$^{\Delta hepa}$/TNFR1$^{-/-}$ animals revealed significantly less vascularised tumor nodules and a decreased liver mass index compared with Nemo$^{\Delta hepa}$ animals (Figures 5a and b). However, despite reduced tumor formation in Nemo$^{\Delta hepa}$/TNFR1$^{-/-}$ mice, the livers of these mice still exhibited some regenerative nodules.

H&E stainings of 1-year-old Nemo$^{\Delta hepa}$ and Nemo$^{\Delta hepa}$/TRAIL$^{-/-}$ mice showed nodules of proliferative hepatocytes with disturbed liver architecture and hepatocellular lipid storage, whereas Nemo$^{\Delta hepa}$/TNFR1$^{-/-}$ showed a more preserved lobular architecture with portal tracts and central veins, diminished hepatocellular lipid storage and mild pleomorphism of hepatocytes (Figure 5b). The impact on lipid accumulation was quantified by Oil Red-O staining (Figure 5c). At this stage, Nemo$^{\Delta hepa}$ and Nemo$^{\Delta hepa}$

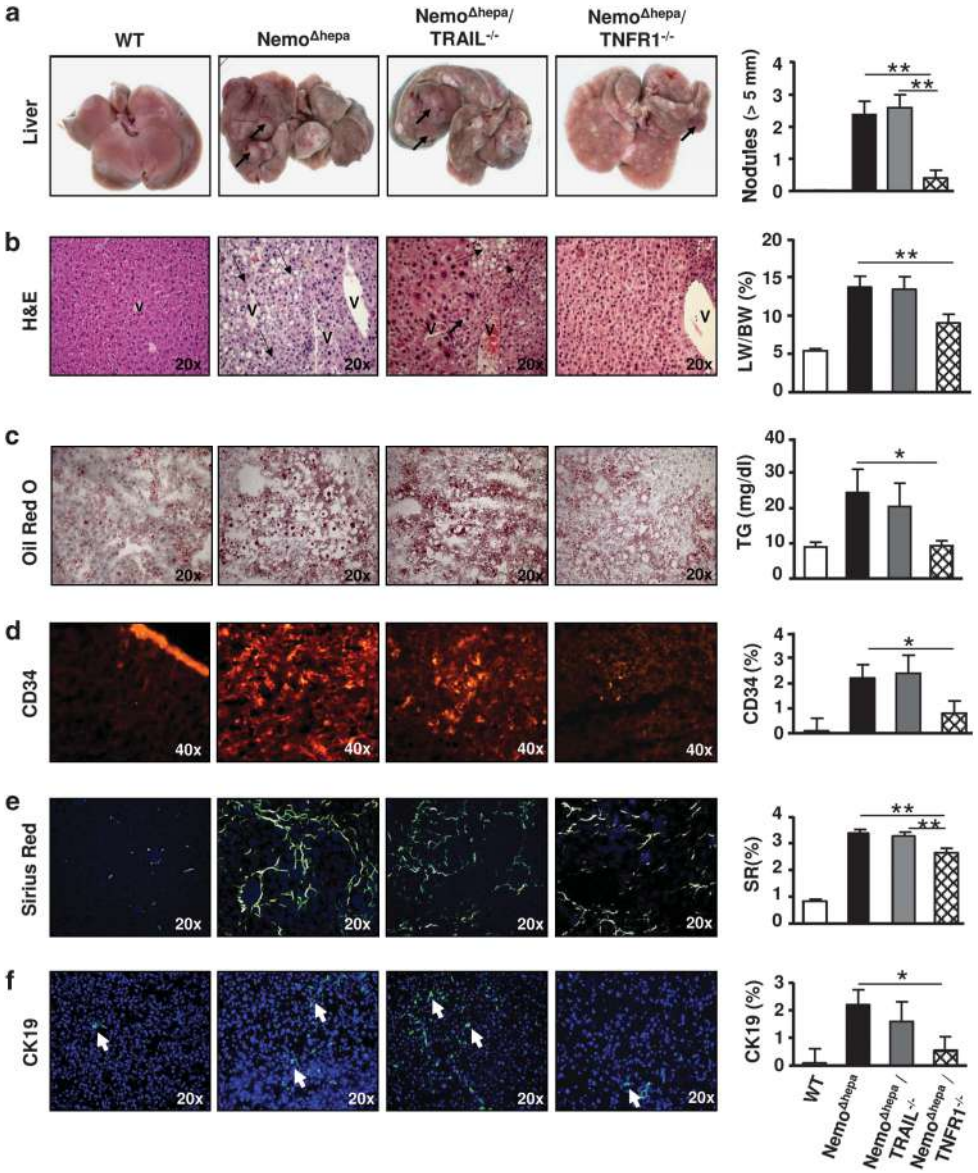

Figure 5 Hepatocarcinogenesis in Nemo$^{\Delta hepa}$ mice can be diminished by blocking TNFR1. WT, Nemo$^{\Delta hepa}$, Nemo$^{\Delta hepa}$/TRAIL$^{-/-}$ and Nemo$^{\Delta hepa}$/TNFR1$^{-/-}$ mice at the age of 12 months were killed and the extracted livers were analyzed macroscopically and by using molecular markers of HCC. (**a**) Macroscopic appearance of livers. Arrows show visible nodules. Number of nodules $\geq$5 mm in diameter were quantified. (**b**) Representative H/E stainings of liver sections. Liver weight *versus* body weight ratio is shown. (**c**) Representative Oil-red-O-stained histological sections in the different mice strains and liver trygliceride content (mg/dl) in these mice strains. (**d**) CD34^{+} immunofluorescence staining in the different mice strains and quantification of positive signal. (**e**) Representative Sirius Red of liver sections, indicating fibrosis and percentage of Sirius Red-positive areas. (**f**) CK19-positive cells were stained in 1-year-old mice. Quantification of CK-19-positive cells ($n=5$). Results are expressed as mean ± S.E.M. ($n=6$–12, $^{*}P<0.05$; $^{**}P<0.01$)

/TRAIL$^{-/-}$ livers showed signs of steatosis, with increased lipid deposition that was not evident in Nemo$^{\Delta hepa}$/TNFR1$^{-/-}$ mice.

The endothelial cell marker CD34 has been used as a clinical tool in the diagnosis of well-differentiated HCC.[16] CD34 staining of 52-week-old Nemo$^{\Delta hepa}$ and Nemo$^{\Delta hepa}$/TRAIL$^{-/-}$ livers revealed a strongly preserved reticulum network within a tumor, which is surrounded by individual tumor cells in a monolayered trabecular pattern, whereas in 1-year-old liver sections of Nemo$^{\Delta hepa}$/TNFR1$^{-/-}$ mice, only a low percentage of CD34-positive cells was detected (Figure 5d).

Next, we tested fibrosis progression in 1-year-old livers. As shown at earlier time points (see Figure 2), ablation of TNFR1–but not of TRAIL – also reduced advanced liver fibrosis in 52-week-old Nemo$^{\Delta hepa}$ mice as demonstrated by quantification of Sirius red-positive areas (Figure 5e). Our earlier results demonstrated that Nemo deficiency triggers hepatitis associated with the proliferation of CK19-positive cells, which mostly represent liver oval stem cells (Figure 5f). Interestingly, the numbers of CK19-positive cells in the Nemo$^{\Delta hepa}$/TNFR1$^{-/-}$ liver were significantly reduced compared with Nemo$^{\Delta hepa}$ livers. Thus, Nemo$^{\Delta hepa}$/TNFR1 mice show reduced overall liver damage and disease

progression (fibrosis and HCC) and consequently a diminished proliferative response in the oval-cell compartment.

Deletion of TNFR1 signaling in Nemo$^{\Delta hepa}$/TRAIL$^{-/-}$ mice reverts liver injury. As the deletion of TRAIL did not change the progression of Nemo$^{\Delta hepa}$-dependent hepatitis, we examined whether TNFR1 deletion in Nemo$^{\Delta hepa}$/TRAIL$^{-/-}$ mice reverts liver injury (Figure 6). Macroscopic examination of Nemo$^{\Delta hepa}$/TRAIL$^{-/-}$/TNFR1$^{-/-}$ triple-knockout livers elicited reduced disease progression compared with Nemo$^{\Delta hepa}$/TRAIL$^{-/-}$ mice (Figure 6a). Liver weight (not shown), the ratio between liver and body weight, and the number of nodules >5.0 mm were similar to Nemo$^{\Delta hepa}$/TNFR1$^{-/-}$ livers and significantly decreased compared with Nemo$^{\Delta hepa}$ and Nemo$^{\Delta hepa}$/TRAIL$^{-/-}$ animals (Figure 6a, right panel, Supplementary Figure 5). H&E stainings revealed reduced macrosteatosis and immune-cell infiltration and serum ALT levels showing that the loss of TNFR1 in Nemo$^{\Delta hepa}$/TRAIL$^{-/-}$ reverted liver injury (Figure 6b). Moreover, the important role of TNFR1 for spontaneous hepatocyte apoptosis was further confirmed in Nemo$^{\Delta hepa}$/TRAIL$^{-/-}$/TNFR1$^{-/-}$ triple-knockout livers showing reduced apoptosis compared with Nemo$^{\Delta hepa}$/TRAIL$^{-/-}$ animals and resembling cell death as found in Nemo$^{\Delta hepa}$/TNFR1$^{-/-}$ livers (Figure 6c). Furthermore, compensatory proliferation and liver fibrogenesis were reduced in Nemo$^{\Delta hepa}$/TRAIL$^{-/-}$/TNFR1$^{-/-}$ triple-knockout livers compared with Nemo$^{\Delta hepa}$/TRAIL$^{-/-}$ but similar to Nemo$^{\Delta hepa}$/TNFR1$^{-/-}$ mice (Figures 6d and e). Taking together, these results support the important role of TNFR1 for the progression of chronic liver injury.

Deletion of TNFR1 in hematopoietic cells promotes acute and chronic liver injuries *in vivo*. As the deletion of TNFR1 in Nemo$^{\Delta hepa}$/TRAIL$^{-/-}$ mice highlights its importance for the progression of chronic liver injury, we next aimed to identify the cell type responsible for this effect. Besides hepatocytes, TNFR1 is expressed in most tissues including liver-infiltrating myeloid cells. To test the relevance of bone-marrow-derived cells, we performed bone marrow transplantation (BMT) experiments in 4–6-week-old mice (Figure 7a). TNFR1$^{-/-}$ bone marrow was transplanted into Nemo$^{\Delta hepa}$ animals (TNFR1$^{-/-}$ → Nemo$^{\Delta hepa}$) as well as into Nemo$^{\Delta hepa}$/TNFR1$^{-/-}$ recipients (TNFR1$^{-/-}$ → Nemo$^{\Delta hepa}$/TNFR1$^{-/-}$) following lethal irradiation. WT mice transplanted with WT bone marrow (WT → WT) and TNFR1$^{-/-}$ mice transplanted with TNFR1$^{-/-}$ (TNFR1$^{-/-}$ → TNFR1$^{-/-}$) were included as controls. In parallel, we transplanted WT bone marrow into Nemo$^{\Delta hepa}$ (WT → Nemo$^{\Delta hepa}$) and Nemo$^{\Delta hepa}$/TNFR1$^{-/-}$ (WT → Nemo$^{\Delta hepa}$/TNFR1$^{-/-}$) animals. As previously published,[17] in order to achieve complete replenishment of the Kupffer-cell population after BMT, we killed the mice, 4 or 48 weeks later, to analyze the contribution of TNFR1 in immune cells to the progression of liver disease (Figure 7a). Chimerism in the liver was confirmed using PCR, which demonstrated successful reconstitution (Figure 7b).

In the acute situation, Nemo$^{\Delta hepa}$ livers 4 weeks after TNFR1$^{-/-}$ bone marrow (TNFR1$^{-/-}$ → Nemo$^{\Delta hepa}$) elicited the presence of immune infiltration, fat deposition, aberrant mitosis and cell death (Figure 7c). This was associated with elevated levels of serum ALT (Figure 7d). Conversely, reconstitution of Nemo$^{\Delta hepa}$ mice with WT bone marrow (WT → Nemo$^{\Delta hepa}$) resulted in no significant histological or serological difference compared with non-reconstituted Nemo$^{\Delta hepa}$ mice (Figure 7c). Reconstitution of double knockouts with WT (WT → Nemo$^{\Delta hepa}$/TNFR1$^{-/-}$) or TNFR1$^{-/-}$ (TNFR1$^{-/-}$ → Nemo$^{\Delta hepa}$/TNFR1$^{-/-}$) bone marrow had no significant effect compared with the non-reconstituted double-knockout mice. These livers were characterized by mild infiltration, steatosis and cell death (Figure 7c).

Finally, we examined the influence of BMT derived from WT- and TNFR1$^{-/-}$ animals on the progression of Nemo$^{\Delta hepa}$-dependent liver injury. We killed chimeric mice 1 year after BMT and evaluated the markers of liver injury and tumorigenesis (Supplementary Figures 6A–C). As observed at the acute time points, Nemo$^{\Delta hepa}$ livers reconstituted with TNFR1$^{-/-}$ bone marrow exhibited strong infiltration, macro- and microsteatosis, and massive hepatitis accompanied by increased levels of alkaline phosphatase (AP) and augmented number of nodules >0.5 cm compared with the other BMT controls included. Altogether, these data suggest that bone-marrow-derived TNFR1 is involved in determining the degree of Nemo$^{\Delta hepa}$-dependent liver injury.

Discussion

In the present study, we demonstrate that the death receptor TNFR1 is crucial in the interplay with IKKγ/Nemo to drive apoptotic cell death of hepatocytes during chronic liver injury. Its cognate ligand TNF is a pleiotropic cytokine produced mainly by KC, NK cells, sinusoidal endothelial cells and hepatic stellate cells, which critically regulate inflammation, cellular injury, cell death/apoptosis and wound healing.

Ligand binding of TNF with TNFR1 triggers formation of the IKK complex and transcription of NF-κB-dependent anti-apoptotic genes. In the absence of the regulatory subunit IKKγ/Nemo, the IKK complex cannot be activated and the canonical NF-κB signaling pathway is blocked, which triggers the Casp8-dependent cell death.[18,19] This is corroborated by the fact that livers of Nemo$^{\Delta hepa}$ mice exhibit spontaneously elevated TNF and TNFR1 levels and therefore show increased hepatocyte apoptosis.[13,20] The impact of IKKγ/Nemo on liver injury is not only relevant in experimental mouse models but also in human disease, as patients with HCC frequently show mutations in the IKKγ/Nemo locus.[21] These findings strongly suggest that results in the IKKγ/Nemo mouse model are useful for the translation of the bench work into clinical studies.

Our results indicate that elevated TNF levels found in Nemo$^{\Delta hepa}$ mice are essential in increasing Casp8 activity and subsequent apoptosis, thereby determining the severe spontaneous phenotype of Nemo$^{\Delta hepa}$ livers. Consequently, Nemo-deficient hepatocytes are more sensitive to TNF and TNF-inducing stimuli such as LPS.[6,7,18] In the present study, we demonstrated that the hypersensitivity of Nemo-deficient hepatocytes towards pro-apoptotic stimulation can be at least partially rescued by genetic TNFR1 inactivation. However, blocking Casp8 in Nemo$^{\Delta hepa}$ hepatocytes completely protected from receptor-mediated apoptosis,[9] suggesting that

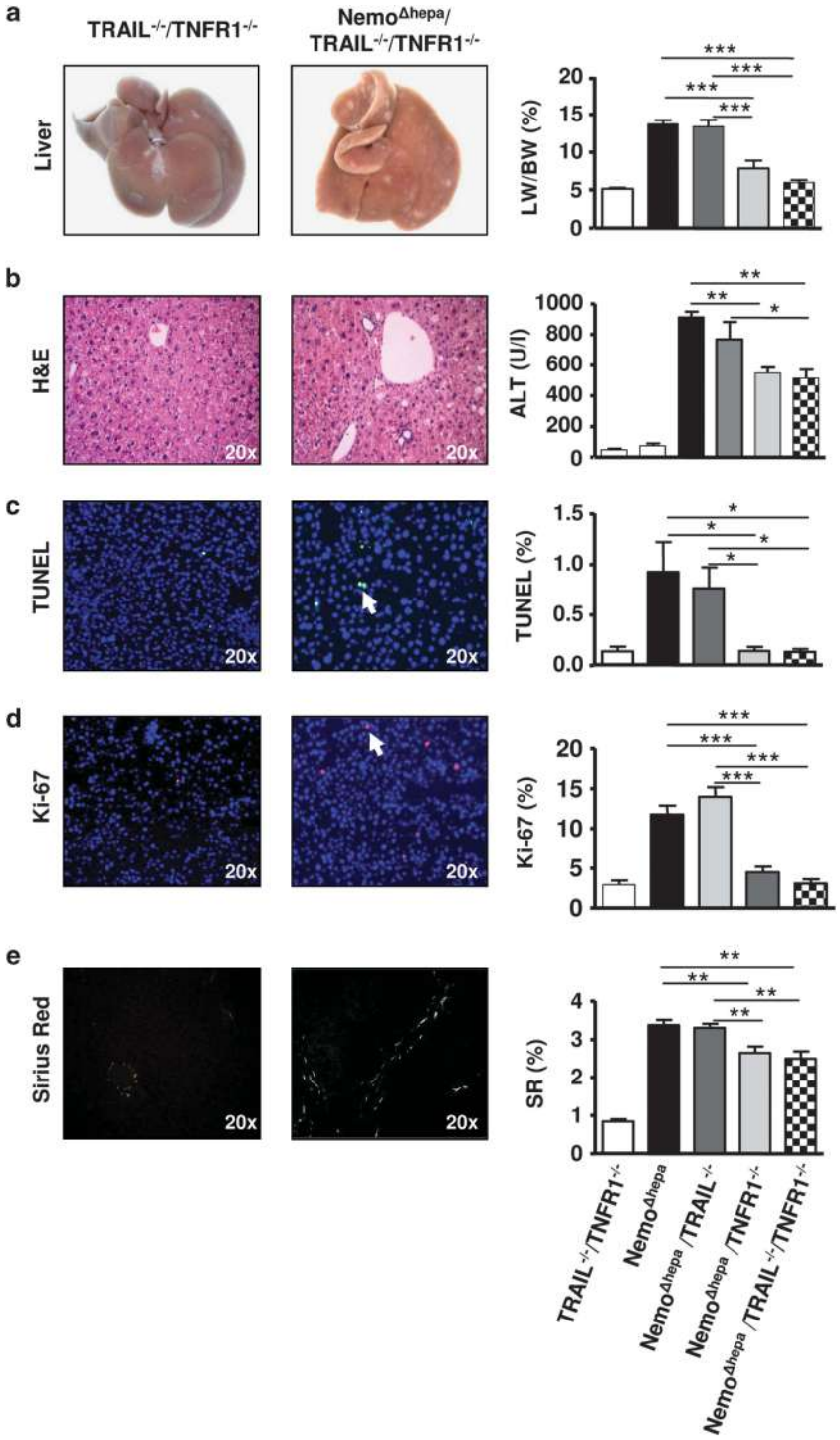

Figure 6 Deletion of TNFR1 signaling in Nemo$^{\Delta hepa}$/TRAIL$^{-/-}$ mice reverts liver injury. (**a**) Macroscopic appearance of livers of TRAIL$^{-/-}$/TNFR1$^{-/-}$ and Nemo$^{\Delta hepa}$/TRAIL$^{-/-}$/TNFR1$^{-/-}$ mice at 8 weeks of age. Liver weight *versus* body weight ratio in TRAIL$^{-/-}$/TNFR1$^{-/-}$ and Nemo$^{\Delta hepa}$/TRAIL$^{-/-}$/TNFR1$^{-/-}$ was compared with Nemo$^{\Delta hepa}$, Nemo$^{\Delta hepa}$/TRAIL$^{-/-}$ and Nemo$^{\Delta hepa}$/TNFR1$^{-/-}$ mice at 8 weeks of age. (**b**) Representative H/E staining of liver sections of 8-week-old TRAIL$^{-/-}$/TNFR1$^{-/-}$ and Nemo$^{\Delta hepa}$/TRAIL$^{-/-}$/TNFR1$^{-/-}$ mice. Serum ALT levels of 8-week-old TRAIL$^{-/-}$/TNFR1$^{-/-}$ and Nemo$^{\Delta hepa}$/TRAIL$^{-/-}$/TNFR1$^{-/-}$ were determined and compared with Nemo$^{\Delta hepa}$, Nemo$^{\Delta hepa}$/TRAIL$^{-/-}$ and Nemo$^{\Delta hepa}$/TNFR1$^{-/-}$ mice at 8 weeks of age. (**c**) Representative TUNEL staining of 8 weeks old liver sections of TRAIL$^{-/-}$/TNFR1$^{-/-}$ and Nemo$^{\Delta hepa}$/TRAIL$^{-/-}$/TNFR1$^{-/-}$. TUNEL-positive cells in these livers were quantified and compared with those of Nemo$^{\Delta hepa}$, Nemo$^{\Delta hepa}$/TRAIL$^{-/-}$ and Nemo$^{\Delta hepa}$/TNFR1$^{-/-}$ mice. (**d**) Representative Ki-67 immunofluorescent staining of liver tissue from 8-week-old TRAIL$^{-/-}$/TNFR1$^{-/-}$ and Nemo$^{\Delta hepa}$/TRAIL$^{-/-}$/TNFR1$^{-/-}$ liver. Quantification of Ki-67-positive cells in these mice was assessed and compared with those of Nemo$^{\Delta hepa}$, Nemo$^{\Delta hepa}$/TRAIL$^{-/-}$ and Nemo$^{\Delta hepa}$/TNFR1$^{-/-}$ mice. (**e**) Representative Sirius red staining of paraffin-embedded liver tissue from 8-week-old livers of TRAIL$^{-/-}$/TNFR1$^{-/-}$ and Nemo$^{\Delta hepa}$/TRAIL$^{-/-}$/TNFR1$^{-/-}$. Image J was used to quantify collagen deposits in these mice that were compared with those of Nemo$^{\Delta hepa}$, Nemo$^{\Delta hepa}$/TRAIL$^{-/-}$ and Nemo$^{\Delta hepa}$/TNFR1$^{-/-}$ mice Values are mean ± S.E.M. from 8–10 mice per group (*$P<0.05$; **$P<0.01$; ***$P<0.001$)

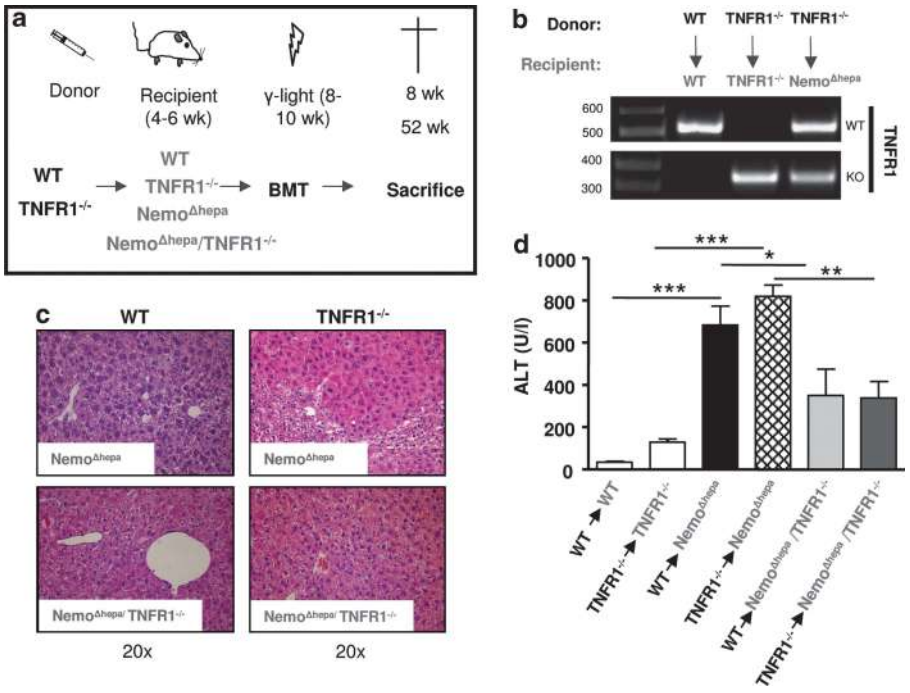

Figure 7 Deletion of TNFR1 in hematopoietic cells is not sufficient to ameliorate liver injury *in vivo*. (**a**) Four to six weeks old Nemo$^{\Delta hepa}$ and Nemo$^{\Delta hepa}$/TNFR1$^{-/-}$ mice were reconstituted with bone marrow from WT and TNFR1$^{-/-}$ mice. Four weeks after transplantation mice were killed and liver samples were collected. (**b**) PCR genotyping obtained from mice 4 weeks after BMT, confirming successful chimerism in the liver. (**c**) Representative H/E staining is shown at $\times 20$ magnification. (**d**) Serum ALT levels of bone marrow-transplanted mice were determined after 4 weeks. Results are expressed as mean; error bars indicate S.E.M. ($n=3$, $^{*}P<0.05$, $^{**}P<0.01$ and $^{***}P<0.001$)

besides TNFR1 additional death receptors contribute to Casp8-dependent liver injury in Nemo$^{\Delta hepa}$ mice.

We have previously shown that Nemo$^{\Delta hepa}$ livers are hypersensitive towards TRAIL stimulation.[13] Therefore, our initial hypothesis was that stable deletion of TRAIL in Nemo$^{\Delta hepa}$ mice would cause a significant improvement of chronic liver injury. Unexpectedly, disease activity in a genetic approach using Nemo$^{\Delta hepa}$/TRAIL$^{-/-}$ double-knockout mice was not ameliorated. Thus, TRAIL-mediated signals are not dominant to determine chronic disease progression in Nemo$^{\Delta hepa}$ livers. However, they become essential to drive the death of Nemo-deficient cells in scenarios of acute but transient injury as reported, for example, after Concanavalin A treatment.[13] To further validate our findings, we generated Nemo$^{\Delta hepa}$/TRAIL$^{-/-}$/TNFR1$^{-/-}$ triple-knockout mice. These animals exhibited the same milder phenotype as Nemo$^{\Delta hepa}$/TNFR1$^{-/-}$ mice, supporting our findings that TNFR1 but not TRAIL is essential to determine chronic injury in Nemo$^{\Delta hepa}$ livers.

Higher pro-inflammatory cytokine levels in Nemo$^{\Delta hepa}$ mice indicate that they are critically involved in the progression of chronic liver injury. In order to better understand the mechanisms ameliorating liver injury in Nemo$^{\Delta hepa}$/TNFR1$^{-/-}$ mice, we performed differential gene-expression profiling from Nemo$^{\Delta hepa}$/TNFR1$^{-/-}$ *versus* Nemo$^{\Delta hepa}$ liver tissue. Interestingly, this analysis revealed that besides others, especially pro-inflammatory cytokines were reduced in Nemo$^{\Delta hepa}$/TNFR1$^{-/-}$ livers. In fact, hepatocyte death activates KC to express cytokines such as TNF and IL-6.[22] In agreement with earlier studies,[23] levels of TNF are downregulated after the deletion of TNFR1, which might contribute to reduced activation and recruitment of immune cells found in Nemo$^{\Delta hepa}$/TNFR1$^{-/-}$ mice.

IL-6 is a multifunctional cytokine largely responsible for the acute-phase response that exerts hepatoprotective effects.[24,25] We reasoned that IL-6 levels are increased in Nemo$^{\Delta hepa}$ mice to counteract hepatocyte damage by inducing hepatic expression of liver-protective proteins such as SAA2.[25,26] In line with this hypothesis, reduced activation of the IL-6/STAT3/SAA2 cascade as found in Nemo$^{\Delta hepa}$/TNFR1$^{-/-}$ mice would be associated with the less-severe liver damage in these animals.

In this context, our data clearly hint at c-Jun N-terminal kinases (JNK) as important downstream mediators of chronic liver injury in Nemo$^{\Delta hepa}$ mice. JNK and JunD activations are induced in Nemo$^{\Delta hepa}$ and Nemo$^{\Delta hepa}$/TRAIL livers, whereas it is inhibited in Nemo$^{\Delta hepa}$ mice lacking TNFR1. Transient and modest JNK activation by TNF is associated with cellular survival, whereas prolonged and robust JNK activation contributes to hepatocyte cell death.[27,28] Transient activation of JNK could be protective, whereas chronic phosphorylation might be pro-apoptotic and thus induce liver damage. Hence, it will be interesting to better define the relevance of JNK for Nemo$^{\Delta hepa}$-dependent liver injury.

Ablation of TNFR1 in Nemo$^{\Delta hepa}$ mice reduced chronic hepatitis characterized by the destruction of liver cells and the persistence of inflammatory cells. Increased apoptosis in Nemo$^{\Delta hepa}$ livers triggers compensatory proliferation of hepatocytes.[8,29] As a consequence, the deletion of TNFR1 decreased cell-death-associated compensatory proliferation and reduced cell cycle activation. Increased chronic liver damage and compensatory proliferation trigger liver fibrosis

in Nemo$^{\Delta hepa}$ mice. TNFR1$^{-/-}$ mice fed with MCD diet, an experimental model of NASH, display less KC activation and decreased fibrosis, associated with reduced collagen deposition. Thus, a role for TNF via TNFR1 in liver fibrosis has been suggested.[30,31] TNFR1 also contributes to spontaneous liver injury, inflammation and fibrosis in hepatocyte-specific TAK1 knockout mice.[32] Previous publications[33] suggest that LPS via the activation of TLR4 and the downregulation of BAMBI is profibrogenic, which could also explain the reduced fibrogenesis in Nemo$^{\Delta hepa}$/TNFR1 livers.

Chronic inflammation increases the risk of cancer development, a characteristic of Nemo$^{\Delta hepa}$ mice.[8] High levels of TNF in these mice contribute to maintain steatohepatitis and subsequently to develop HCC. Tumor progression has been linked to oval-cell proliferation commonly seen in the preneoplastic stages of liver carcinogenesis and often accompanied by an inflammatory response.[34] Nemo$^{\Delta hepa}$ mice show strong activation of the oval-cell compartment to compensate hepatocyte death. After TNFR1 deletion, the oval-cell response as well as the tumor growth in Nemo$^{\Delta hepa}$/TNFR1$^{-/-}$ livers are decreased. Our observations are in agreement with current literature[34–37] strongly suggesting that TNFR1 deficiency is crucial for tumor promotion. A recent paper suggests that TNFR1 ablation, in contrast to IL-6 and MyD88, has no significant effect on hepatocarcinogenesis in the DEN model.[25] However, the same group showed that TNFR1 ablation almost completely abolished obesity-enhanced HCC development.[38] Altogether, these data suggest that TNFR1 may especially have a crucial role in NASH/inflammation-triggered tumorigenesis by exerting an essential effect on liver injury.

From our data we hypothesized that in Nemo$^{\Delta hepa}$ livers, infiltrating hematopoietic cells are an essential source of TNF, whereas Nemo-deficient hepatocytes are the main TNFR1-expressing target cells. In order to better support this hypothesis, we generated chimeras with TNFR1$^{-/-}$ bone marrow in Nemo$^{\Delta hepa}$ and Nemo$^{\Delta hepa}$/TNFR1$^{-/-}$ recipients including their respective controls. Acute and long-term experiments demonstrated that the deletion of TNFR1 in infiltrating immune cells promoted acute and chronic liver diseases in Nemo$^{\Delta hepa}$ mice. It is tempting to speculate that higher phosphorylation levels of STAT3 observed in TNFR1$^{-/-}$ mice might in part be linked to this finding, as it is neutralised in Nemo$^{\Delta hepa}$/TNFR1$^{-/-}$ mice. Our current model derived from these data is illustrated in Figure 8. In agreement with our previous publications,[8] Nemo$^{\Delta hepa}$ mice show high levels of pro-inflammatory cytokines (TNF, IL-6) that increases liver injury by activating TNFR1-dependent apoptosis in hepatocytes.

Moreover, our data suggest that TNFR1 deficiency in immune cells deteriorates Nemo$^{\Delta hepa}$-induced liver injury. Consequently, these findings have major clinical implications. Targeting TNF and TNF receptor for disease intervention is already established for autoimmune and inflammatory disorders.[39] Earlier clinical studies evaluated the promising use of anti-TNF antibodies in alcoholic steatohepatitis (ASH).[40] However, subsequent clinical trials with higher anti-TNF concentrations failed to have a positive effect in these patients and the studies were terminated.[41] Indeed, a primary challenge will be to achieve specificity and efficacy without having any undesirable effects. Here, cell-specific targeting could be a promising approach to improve the clinical outcome of TNF-driven diseases.

In summary, modulating the function of IKKγ/Nemo in mice and humans has been linked to chronic liver injury and HCC development. In the present study, we show that deletion of TNFR1 in hepatocytes is protective, whereas TNFR1 inactivation in bone-marrow-derived cells might be harmful in the context of Nemo$^{\Delta hepa}$-dependent liver injury. Thus, our data suggest that the cell-specific role of TNF-dependent signaling should be considered to optimise future therapeutic strategies.

Materials and Methods

Housing and generation of knockout mice. Animals were maintained in the animal facility of the University Hospital RWTH Aachen according to the German legal requirements. Hepatocyte-specific IKKγ/Nemo mice were generated by crossing loxP site-flanked (floxed [f]) Nemo gene (Nemo$^{f/f}$) with alfp-cre transgenic animals as described before.[13] These mice were further crossed either with TRAIL/DR5 knockout mice, provided by S Bronk (Mayo Clinic College of Medicine, Rochester, MN, USA) to yield Nemo$^{\Delta hepa}$/TRAIL$^{-/-}$ or with TNFR1$^{-/-}$ mice (purchased from The Jackson Laboratory, Bar Harbor, ME, USA) to yield Nemo$^{\Delta hepa}$/TNFR1$^{-/-}$. Finally, we crossed Nemo$^{\Delta hepa}$/TRAIL$^{-/-}$ with TNFR1$^{-/-}$ mice to further generate Nemo$^{\Delta hepa}$/TRAIL$^{-/-}$/TNFR1$^{-/-}$ and investigate the deletion of TNFR1$^{-/-}$ in Nemo$^{\Delta hepa}$/TRAIL$^{-/-}$ mice. To use the proper controls, Nemo$^{\Delta hepa}$ mice were backcrossed from Nemo$^{\Delta hepa}$/TRAIL$^{-/-}$, Nemo$^{\Delta hepa}$/TNFR1$^{-/-}$ and Nemo$^{\Delta hepa}$/TRAIL$^{-/-}$/TNFR1$^{-/-}$. Finally, TRAIL$^{-/-}$/TNFR1$^{-/-}$ were also used as controls. Genotypes were confirmed via PCR specific for the respective alleles using DNA from tail biopsies. Progression of liver disease was investigated in male mice between 8–9 weeks and 52–54 weeks of age. Liver injury experiments were performed on mice between 8 and 9 weeks of age. Serum AST and ALT were measured by the standard procedures in the Institute of Clinical Chemistry, University Hospital, RWTH-Aachen.

TUNEL assay, BrdU assay and caspase-3/8 assay. TUNEL test and BrdU staining were performed by the standard procedures. Caspase-3 and Caspase-8 were measured by using Ac-DEVD-AFC and Ac-IETD-AFC as fluorescent substrates (Biomol GmbH, Hamburg, Germany). Frozen livers were homogenized in ice-cold lysis buffer (1 mol/l HEPES, 10% 3-[(3-cholamidopropyl)-dimethylammonio]-1-propanesulfonate, 0.5 mol/l EDTA, 1 mol/l dithiothreitol and 0.1 mol/l Pefabloc), and protein lysates were incubated with either Ac-DEVD-AFC or Ac-IETD-AFC at 37 °C. After 1 h, the kinetics of enzymatic activity was measured in a luminescence spectrophotometer at a λ excitation of 390 nm and λ emission of 510 nm.

Bone marrow transplantation. We transferred bone marrow of TNFR1$^{-/-}$ or WT mice ($n = 7$–8 mice per group) into 4–6-week-old recipients (isogenic on a C57BL/6J background) after ablative γ-irradiation, as described previously.[42] After 8–10 weeks and 1 year, mice were killed, and liver and serum samples were collected.

Microarray analysis. Affymetrix Microarray data have been deposited with the NCBI Gene Expression Omnibus (http://www.ncbi.nlm.nih.gov/geo/) under the accession number GSE3316. RNA was isolated from mouse livers using TRIzol reagent and purified with the RNeasy Mini Kit (Qiagen, Venlo, The Netherlands) according to the manufacturer's instructions. Concentrations and purity of RNA samples were determined on a NanoDrop ND-1000 spectrophotometer (Isogen, Maarssen, The Netherlands). RNA integrity was checked on an Agilent 2100 bioanalyzer (Agilent Technologies, Amsterdam, The Netherlands) with 6000 Nano Chips. RNA samples from three mice per experimental group were used for microarray analysis. Samples were hybridized on the Affymetrix GeneChip Mouse Genome 430 2.0 arrays in the microarray core laboratory of the Nutrigenomics Consortium at Wageningen University, The Netherlands. Hybridization, washing and scanning of the arrays were performed according to standard Affymetrix protocols. Array images were processed using packages from the Bioconductor

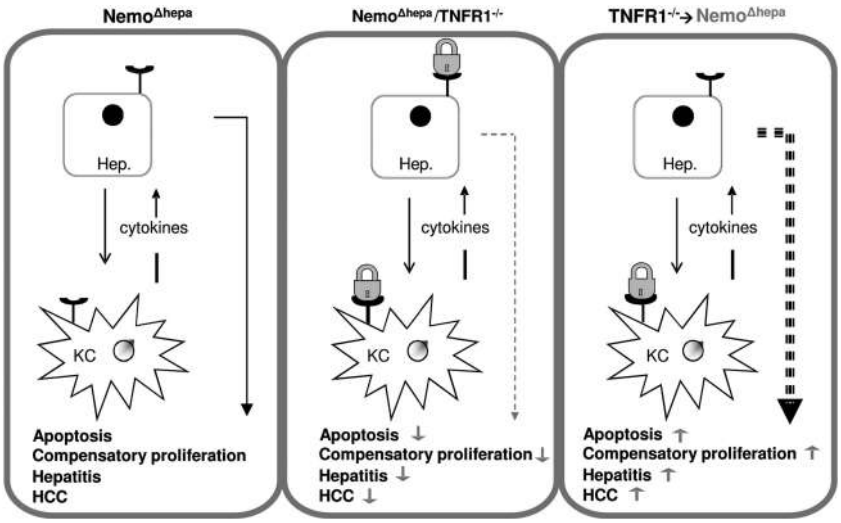

Figure 8 Proposed model for the activation of TNFR1-signaling cascade. In Nemo$^{\Delta hepa}$ mice hepatocyte apoptosis promotes an inflammatory environment that activates Kupffer cells, which release cytokines such as TNF triggering compensatory proliferation, hepatitis and tumor development. In the absence of TNFR1 in hepatocytes, acute and chronic liver injuries are ameliorated. Nemo$^{\Delta hepa}$ chimeric mice reconstituted with TNFR1$^{-/-}$ bone marrow show that TNFR1 activation is crucial in hepatocytes but also in bone-marrow-derived cells. Immune cells lacking TNFR1 promote the development of liver injury in Nemo$^{\Delta hepa}$ mice

project.[43] Probe sets were redefined according to Dai.[44] Probes were assigned to unique gene identifiers, in this case Entrez IDs. Arrays were normalized by quantile normalization and expression estimates were calculated using GC robust multiarray average background adjustment.[45] Differentially expressed genes were identified using linear models with application of moderated *t*-statistics that implement empirical Bayes regularization of standard errors.[46] Genes that satisfied the criteria of a *P*-value of less than 0.01 and fold change greater than 2 were considered to be expressed differentially. Detailed descriptions of the applied methods are available on request.

Primary hepatocyte culture. Primary hepatocytes were prepared by perfusing the portal vein of the liver with EBSS containing 100 mM EGTA (pH 8.3), followed by an EBSS solution containing 20 mg Collagenase D and 2 mg Trypsin inhibitor. Hepatocytes (1×10^6/well) were cultured in Dulbecco's modified medium with 10% FBS, 2 mM L-glutamine and antibiotics on six-well plates with pre-coated and PBS-washed 2.5 mg/ml type I collagen.

Immunoblot and protein analyses. Protein extracts were electrophoresed and then blotted following standard procedures. Blots were incubated with primary antibodies for cleaved Caspase 3 (Cell Signaling Technology, New England Biolabs GmbH, Frankfurt, Germany), phospho-JNK (Cell Signaling Technology), Cyclin A (Santa Cruz Biotechnology, Heidelberg, Germany), p21 (Santa Cruz Biotechnology), PCNA (Cell Signaling Technology) phospho JunD (Ser100) (Cell Signaling Technology), Collagen 1 (Monosan, Uden, The Netherlands), α-SMA (Cymbos Biotech, Hofheim, Germany), p-STAT3 (Cell Signaling Technology) and TNFR1 (Santa Cruz Biotechnology). As a loading control, we used total Caspase 3 (Cell Signaling Technology), total STAT3 (Santa Cruz Biotechnology) and β-actin antibody (Sigma-Aldrich GmbH, Munich, Germany). We used anti-rabbit IgG-HRP-linked (Cell Signaling Biotechnology) and anti-mouse IgG-HRP-linked (Santa Cruz Biotechnology) as secondary antibodies. Analysis of intrahepatic IL-6 was performed in duplicate using a murine ELISA (BD Biosciences, Heidelberg, Germany).

Quantitative real-time PCR. Total RNA was purified from liver tissues using Trizol reagent (Invitrogen, Karlsruhe, Germany). Total RNA (1 μg) was used to synthesize cDNA using SuperScript first-Stand Synthesis System (Invitrogen) and was resuspended in 100 μl of H_2O. Quantitative real time PCR was performed using SYBR Green Reagent (Invitrogen) in 7300 Real Time PCR system (Applied Biosystem, Darmstadt, Germany). GAPDH expression was used to normalize gene expression, which is represented as times *versus* WT basal expression. Primer sequences can be provided upon request.

Histological, immunofluorescence and immunohistochemical analyses. Livers from mice were harvested and, after fixation with 4% PFA, were embedded in paraffin for further histological evaluation. H&E, Oil-Red-O and Sirius Red staining were performed on liver sections. For immunofluorescence analysis, liver cryosections of 5 μm were stained with rat anti-mouse CD11b, rat anti-mouse F4/80, rat anti-mouse Ly6G and rat anti-mouse Ki-67 (all from BD Biosciences). Slides were fixed in 4% PFA at room temperature. Secondary antibody conjugated with FITC, Cy3 (Jackson Immunoresearch, West Grove, PA, USA) was used to obtain green and red fluorescence signals. Mounting solution containing DAPI (Vector Laboratories, Burlingame, CA, USA) was used to counterstain the nuclei of hepatocytes. Paraffin tissue sections from the mouse liver were deparaffinized and rehydrated. After antigen retrieval, sections were incubated overnight at 4 °C with primary biotin-anti-mouse CD45 (clone 30E11; Pharmingen, Heidelberg, Germany) diluted in TBS buffer containing 1% BSA and 0.1% Tween 20. Thereafter, the sections were incubated with streptavidin ABC-alkaline phosphatase (Vector Laboratories) and color was developed with Vector red staining kit (Vector Laboratories) followed by hematoxylin counterstaining.

Flow cytometry analysis. Hepatocytes were stained with Annexin V-FITC (BD Biosciences). Immune cells from whole liver were isolated and stained with fluorochrome-conjugated antibodies (CD4-PE, CD8-FITC, CD45-APC-Cy7, CD11b-PE, Ly6G-FITC and F4/80 Biotin) (BD Biosciences). All samples were acquired by flow cytometry (FACS Canto II; BD Biosciences) and analyzed using the Flowjo software (Ashland, OR, USA).

Statistical analysis. Data are expressed as the mean ± S.D. Statistical significance was determined via two-way analysis of variance followed by Student's *t*-test.

Conflict of Interest

The authors declare no conflict of interest.

Acknowledgements. This work was supported by a grant from the IZKF Aachen (Interdisciplinary Centre for Clinical Research within the faculty of Medicine at the RWTH Aachen University) and the Deutsche Forschungsgemeinschaft (SFB/TRR 57). We would also like to acknowledge Dr. Tom Luedde (Department of Internal Medicine III, University Hospital, RWTH Aachen) and Dr. Mathias Heikenwälder (Institute of Virology, TU Munich) for their thoughtful comments and constructive critique. This paper is dedicated on the occasion of the 60th birthday of Professor Dr. Michael P Manns.

1. Karin M, Lin A. NF-kappaB at the crossroads of life and death. *Nat Immunol* 2002; **3**: 221–227.
2. Pahl HL. Activators and target genes of Rel/NF-kappaB transcription factors. *Oncogene* 1999; **18**: 6853–6866.
3. Schmidt-Supprian M, Bloch W, Courtois G, Addicks K, Israel A, Rajewsky K *et al.* NEMO /IKK gamma-deficient mice model incontinentia pigmenti. *Mol Cell* 2000; **5**: 981–992.
4. Li Q, Van Antwerp D, Mercurio F, Lee KF, Verma IM. Severe liver degeneration in mice lacking the IkappaB kinase 2 gene. *Science* 1999; **284**: 321–325.
5. Tanaka M, Fuentes ME, Yamaguchi K, Durnin MH, Dalrymple SA, Hardy KL *et al.* Embryonic lethality, liver degeneration, and impaired NF-kappa B activation in IKK-beta-deficient mice. *Immunity* 1999; **10**: 421–429.
6. Rudolph D, Yeh WC, Wakeham A, Rudolph B, Nallainathan D, Potter J *et al.* Severe liver degeneration and lack of NF-kappaB activation in NEMO/IKKgamma-deficient mice. *Genes Dev* 2000; **14**: 854–862.
7. Beraza N, Ludde T, Assmus U, Roskams T, Vander Borght S, Trautwein C. Hepatocyte-specific IKK gamma/NEMO expression determines the degree of liver injury. *Gastroenterology* 2007; **132**: 2504–2517.
8. Luedde T, Beraza N, Kotsikoris V, van Loo G, Nenci A, De Vos R *et al.* Deletion of NEMO /IKKgamma in liver parenchymal cells causes steatohepatitis and hepatocellular carcinoma. *Cancer Cell* 2007; **11**: 119–132.
9. Liedtke C, Bangen JM, Freimuth J, Beraza N, Lambertz D, Cubero FJ *et al.* Loss of caspase-8 protects mice against inflammation-related hepatocarcinogenesis but induces non-apoptotic liver injury. *Gastroenterology* 2011; **141**: 2176–2187.
10. Papa S, Bubici C, Zazzeroni F, Franzoso G. Mechanisms of liver disease: cross-talk between the NF-kappaB and JNK pathways. *Biol Chem* 2009; **390**: 965–976.
11. Doi TS, Marino MW, Takahashi T, Yoshida T, Sakakura T, Old LJ *et al.* Absence of tumor necrosis factor rescues RelA-deficient mice from embryonic lethality. *Proc Natl Acad Sci USA* 1999; **96**: 2994–2999.
12. Rosenfeld ME, Prichard L, Shiojiri N, Fausto N. Prevention of hepatic apoptosis and embryonic lethality in RelA/TNFR-1 double knockout mice. *Am J Pathol* 2000; **156**: 997–1007.
13. Beraza N, Malato Y, Sander LE, Al-Masaoudi M, Freimuth J, Riethmacher D *et al.* Hepatocyte-specific NEMO deletion promotes NK/NKT cell- and TRAIL-dependent liver damage. *J Exp Med* 2009; **206**: 1727–1737.
14. Kwon YH, Jovanovic A, Serfas MS, Tyner AL. The Cdk inhibitor p21 is required for necrosis, but it inhibits apoptosis following toxin-induced liver injury. *J Biol Chem* 2003; **278**: 30348–30355.
15. Karlmark KR, Wasmuth HE, Trautwein C, Tacke F. Chemokine-directed immune cell infiltration in acute and chronic liver disease. *Expert Rev Gastroenterol Hepatol* 2008; **2**: 233–242.
16. Onofre AS, Pomjanski N, Buckstegge B, Bocking A. Immunocytochemical diagnosis of hepatocellular carcinoma and identification of carcinomas of unknown primary metastatic to the liver on fine-needle aspiration cytologies. *Cancer* 2007; **111**: 259–268.
17. Klein I, Cornejo JC, Polakos NK, John B, Wuensch SA, Topham DJ *et al.* Kupffer cell heterogeneity: functional properties of bone marrow derived and sessile hepatic macrophages. *Blood* 2007; **110**: 4077–4085.
18. Legarda-Addison D, Hase H, O'Donnell MA, Ting AT. NEMO/IKKgamma regulates an early NF-kappaB-independent cell-death checkpoint during TNF signaling. *Cell Death Differ* 2009; **16**: 1279–1288.
19. Yamaoka S, Courtois G, Bessia C, Whiteside ST, Weil R, Agou F *et al.* Complementation cloning of NEMO, a component of the IkappaB kinase complex essential for NF-kappaB activation. *Cell* 1998; **93**: 1231–1240.
20. Chaisson ML, Brooling JT, Ladiges W, Tsai S, Fausto N. Hepatocyte-specific inhibition of NF-kappaB leads to apoptosis after TNF treatment, but not after partial hepatectomy. *J Clin Invest* 2002; **110**: 193–202.
21. Aigelsreiter A, Haybaeck J, Schauer S, Kiesslich T, Bettermann K, Griessbacher A *et al.* NEMO expression in human hepatocellular carcinoma and its association with clinical outcome. *Hum Pathol* 2012; **43**: 1012–1019.
22. Canbay A, Gieseler RK, Gores GJ, Gerken G. The relationship between apoptosis and non-alcoholic fatty liver disease: an evolutionary cornerstone turned pathogenic. *Z Gastroenterol* 2005; **43**: 211–217.
23. Guo G, Morrissey J, McCracken R, Tolley T, Klahr S. Role of TNFR1 and TNFR2 receptors in tubulointerstitial fibrosis of obstructive nephropathy. *Am J Physiol* 1999; **277**(5 Pt 2): F766–F772.
24. Klein C, Wustefeld T, Assmus U, Roskams T, Rose-John S, Muller M *et al.* The IL-6-gp 130-STAT3 pathway in hepatocytes triggers liver protection in T cell-mediated liver injury. *J Clin Invest* 2005; **115**: 860–869.
25. Naugler WE, Sakurai T, Kim S, Maeda S, Kim K, Elsharkawy AM *et al.* Gender disparity in liver cancer due to sex differences in MyD88-dependent IL-6 production. *Science* 2007; **317**: 121–124.
26. Gao B. Cytokines, STATs and liver disease. *Cell Mol Immunol* 2005; **2**: 92–100.
27. De Smaele E, Zazzeroni F, Papa S, Nguyen DU, Jin R, Jones J *et al.* Induction of gadd45beta by NF-kappaB downregulates pro-apoptotic JNK signaling. *Nature* 2001; **414**: 308–313.
28. Tang G, Minemoto Y, Dibling B, Purcell NH, Li Z, Karin M *et al.* Inhibition of JNK activation through NF-kappaB target genes. *Nature* 2001; **414**: 313–317.
29. Weber A, Boege Y, Reisinger F, Heikenwalder M. Chronic liver inflammation and hepatocellular carcinoma: persistence matters. *Swiss Med Wkly* 2011; **141**: w13197.
30. Tarrats N, Moles A, Morales A, Garcia-Ruiz C, Fernandez-Checa JC, Mari M. Critical role of tumor necrosis factor receptor 1, but not 2, in hepatic stellate cell proliferation, extracellular matrix remodeling, and liver fibrogenesis. *Hepatology* 2011; **54**: 319–327.
31. Li Z, Yang S, Lin H, Huang J, Watkins PA, Moser AB *et al.* Probiotics and antibodies to TNF inhibit inflammatory activity and improve nonalcoholic fatty liver disease. *Hepatology* 2003; **37**: 343–350.
32. Inokuchi S, Aoyama T, Miura K, Osterreicher CH, Kodama Y, Miyai K *et al.* Disruption of TAK1 in hepatocytes causes hepatic injury, inflammation, fibrosis, and carcinogenesis. *Proc Natl Acad Sci USA* 2010; **107**: 844–849.
33. Seki E, De Minicis S, Osterreicher CH, Kluwe J, Osawa Y, Brenner DA *et al.* TLR4 enhances TGF-beta signaling and hepatic fibrosis. *Nat Med* 2007; **13**: 1324–1332.
34. Knight B, Yeoh GC, Husk KL, Ly T, Abraham LJ, Yu C *et al.* Impaired preneoplastic changes and liver tumor formation in tumor necrosis factor receptor type 1 knockout mice. *J Exp Med* 2000; **192**: 1809–1818.
35. Yamada Y, Kirillova I, Peschon JJ, Fausto N. Initiation of liver growth by tumor necrosis factor: deficient liver regeneration in mice lacking type I tumor necrosis factor receptor. *Proc Natl Acad Sci USA* 1997; **94**: 1441–1446.
36. Yamada Y, Webber EM, Kirillova I, Peschon JJ, Fausto N. Analysis of liver regeneration in mice lacking type 1 or type 2 tumor necrosis factor receptor: requirement for type 1 but not type 2 receptor. *Hepatology* 1998; **28**: 959–970.
37. Yamada Y, Fausto N. Deficient liver regeneration after carbon tetrachloride injury in mice lacking type 1 but not type 2 tumor necrosis factor receptor. *Am J Pathol* 1998; **152**: 1577–1589.
38. Park EJ, Lee JH, Yu GY, He G, Ali SR, Holzer RG *et al.* Dietary and genetic obesity promote liver inflammation and tumorigenesis by enhancing IL-6 and TNF expression. *Cell* 2010; **140**: 197–208.
39. Croft M, Benedict CA, Ware CF. Clinical targeting of the TNF and TNFR superfamilies. *Nat Rev Drug Discov* 2013; **12**: 147–168.
40. Tilg H, Vogelsang H, Ludwiczek O, Lochs H, Kaser A, Colombel JF *et al.* A randomised placebo controlled trial of pegylated interferon alpha in active ulcerative colitis. *Gut* 2003; **52**: 1728–1733.
41. Naveau S, Chollet-Martin S, Dharancy S, Mathurin P, Jouet P, Piquet MA *et al.* A double-blind randomized controlled trial of infliximab associated with prednisolone in acute alcoholic hepatitis. *Hepatology* 2004; **39**: 1390–1397.
42. Berres ML, Trautwein C, Schmeding M, Eurich D, Tacke F, Bahra M *et al.* Serum chemokine CXC ligand 10 (CXCL10) predicts fibrosis progression after liver transplantation for hepatitis C infection. *Hepatology* 2011; **53**: 596–603.
43. Gentleman RC, Carey VJ, Bates DM, Bolstad B, Dettling M, Dudoit S *et al.* Bioconductor: open software development for computational biology and bioinformatics. *Genome Biol* 2004; **5**: R80.
44. Dai M, Wang P, Boyd AD, Kostov G, Athey B, Jones EG *et al.* Evolving gene/transcript definitions significantly alter the interpretation of GeneChip data. *Nucleic Acids Res* 2005; **33**: e175.
45. Wu Z, Irizarry RA. Preprocessing of oligonucleotide array data. *Nat Biotechnol* 2004; **22**: 656–658; Author reply 658.
46. Smyth GK. Linear models and empirical bayes methods for assessing differential expression in microarray experiments. *Stat Appl Genet Mol Biol* 2004; **3**: 1–26.

Supplementary Information accompanies this paper on Cell Death and Differentiation website (http://www.nature.com/cdd)